Journal of Solid State Chemistry 185 (2012) 117–123

Contents lists available at SciVerse ScienceDirect

Journal of Solid State Chemistry

journal homepage: www.elsevier.com/locate/jssc

Hematite homogeneous core/shell hierarchical spheres: Surfactant-free solvothermal preparation and their improved catalytic property of selective oxidation

Suoyuan Lian [a,b], Haitao Li [a], Xiaodie He [a], Zhenhui Kang [a,*], Yang Liu [a,*], Shuit Tong Lee [a]

[a] Institute of Functional Nano & Soft Materials and Jiangsu Key Laboratory for Carbon-Based Functional Materials & Devices, Soochow University, Box 32, 199 Ren-ai Road, Suzhou Industrial Park, Suzhou 215123, China
[b] School of Chemical Engineering & Materials, Dalian Polytechnic University, Dalian 116034, China

ARTICLE INFO

Article history:
Received 24 August 2011
Received in revised form
31 October 2011
Accepted 2 November 2011
Available online 11 November 2011

Keywords:
Iron oxide
Alcoholysis
Alcohol oxidation
Catalyst
Selectivity

ABSTRACT

Solvothermal synthesis is an efficient synthetic method for preparing nano and micromaterials. Preparation of hematite through alcoholysis of ferric ion under solvothermal condition has been carried out at low concentrations. In this paper, Fe_2O_3 homogeneous core/shell hierarchical nanostructures were synthesized via solvothermal treatment of $FeCl_3 \cdot 6H_2O$ and ethanol. The achievements of such structures can be attributed to two important factors: high temperature and high concentration. Besides, the crystal water and reaction time were also important factors to the synthesis of hematite. The prepared samples were characterized using X-ray powder diffraction, Raman spectra, scanning electron microscopy equipped with an energy-dispersive X-ray spectrometer, transmission electron microscopy and Brunauer–Emmett–Teller surface area and pore size distribution. X-ray photoelectron spectroscopy showed a satellite peak at 719.8 eV, which is the characteristic peak of Fe(III). The formation mechanism of the spheres and the effects of the reactant concentrations and reaction temperatures have been discussed. Moreover, the enhanced catalytic activity of the spheres has also been investigated through oxidation of benzyl alcohol to benzaldehyde with high conversion (42%) and selectivity (95%).

1. Introduction

In recent years, inorganic core/shell nanostructures or microstructures have attracted much attention owning to their unique structures and interesting properties, such as applications in optical, electronic, magnetic, catalytic and sensing devices [1–7]. Most core/shell nanostructures were generally composed of two completely different materials [8,9], of which act as the core and the shell, respectively. Therefore such materials were usually called "heterogeneous core/shell nanostructures". On the contrary, "homogeneous core/shell nanostructures" means the same material for both the core and the shell. Comparing with heterogeneous core/shell nanostructures, it seems much more difficult to obtain the homogeneous core/shell nanostructures, because the core and shell usually grow as a whole with the same substance. Up to present, there are only a few examples that have been reported on the preparation of core/shell nanostructures [10–15]. Recently, some groups have synthesized γ-Fe_2O_3 and α-Fe_2O_3 core/shell structures, which were self-assembled by nanosheets through iron compound as precursor with thermal treatment [16,17]. However, their preparation steps are complicated and need high temperature.

On the other hand, different materials possess different features based on the microscopic structures. Iron oxides, which are environmentally benign with low toxicity and price, have many practical applications [18]. In this family, hematite (α-Fe_2O_3), an environmentally friendly *n*-type semiconductor with a band gap of 2.2 eV, is widely used in catalysts, magnetic materials, pigments, sensors and lithium-ion batteries. Moreover, it is also used as the raw material for the synthesis of magnetic γ-Fe_2O_3, which is of great importance as a ferrofluid and magnetic recording materials [19–22]. Among all the applications, catalysis, especially for selective oxidation, is the most important one and constitutes the industrial core technologies for converting bulk chemicals to useful products of high oxidation state [23,24]. For instance, iron oxide has been developed for alcohol and olefin oxidation [25,26], coupling [27], borylation [28], alkylation [29] and acylation [30]. Up to now, a variety of α-Fe_2O_3 morphologies have been fabricated, such as rhombohedra [31], particles [32], nanocubes [33–35], rings [36,37], wires [38,39], rods [40–43], tubes [44–46], fibers [47], flakes [48,49], cages [50], flower

* Corresponding authors. Fax: +86 512 65882846.
E-mail addresses: zhkang@suda.edu.cn (Z. Kang), yangl@suda.edu.cn (Y. Liu).

0022-4596/$ - see front matter © 2011 Elsevier Inc. All rights reserved.
doi:10.1016/j.jssc.2011.11.003

[51,52], hierarchical structures [53–55] and hollow structures [56–59]. Generally speaking, the simplest synthetic route to core/shell nanostructures is probably self-assembly, in which ordered aggregates are formed in a spontaneous process [60]. However, it is still a big challenge to develop simple and reliable synthetic methods for hierarchically self-assembled architectures with designed chemical components and controlled morphologies, which strongly affect the properties of nanomaterials.

In this paper, homogeneous hematite core/shell hierarchical spheres with diameters of ~4 μm and shell thickness of ~300 nm were fabricated through a facile one-pot solvothermal reaction with $FeCl_3 \cdot 6H_2O$ and ethanol as reactants at 180 °C for 24 h. The average pore size and the BET surface area of the products were 3.5 nm and 23.6 m^2/g, respectively. Ethanol acts as both solvent and reactant, providing water through dehydration. The formation of hematite core/shell structures can be contributed to the self-assembly of hematite nanoparticles, which was controlled by synergistic effects, including reaction time, concentrations, reaction temperatures, and water contents. A possible growth mechanism of the core/shell structure is proposed. In addition, as an example of potential applications, the as-prepared iron oxide nanomaterials are used as catalysts in the oxidation of benzyl alcohol to benzaldehyde with 42% conversion and 95% selectivity.

2. Material and methods

2.1. Reagents and synthesis

$FeCl_3 \cdot 6H_2O$, absolute ethanol, benzyl alcohol, benzaldehyde, benzoic acid, 1,4-dioxane, 30% H_2O_2, bulk hematite and magnetite were all purchased from China National Pharmaceutical Group Corporation and used as received without further purification. Deionized water was used throughout all experiments. Self-assembled homogeneous hematite core/shell hierarchical structures were synthesized via solvothermal treatment of $FeCl_3 \cdot 6H_2O$ dissolved in ethanol. In a typical synthesis procedure, 2–6 g $FeCl_3 \cdot 6H_2O$ was dissolved in 10 mL ethanol, then the solution was transferred into an 18 mL teflon autoclave, which was sealed and heated to 180 °C for 1–20 h, respectively. The products were collected after cooling to room temperature. Then, they were purified by centrifugation–redispersion cycles with ethanol and deionized water for 5 times, and dried in air at 50 °C. The detailed conditions for preparing some typical samples are listed in Table 1.

2.2. Characterization

The as-prepared samples were characterized using X-ray powder diffraction (XRD) (Rigaku D/max 2550 V, Cu$K\alpha$, $\lambda = 1.54178$ Å), scanning electron microscopy (SEM) (Philips XL30 FEG) coupled with an energy-dispersive X-ray (EDX, Oxford Instrument) spectrometer and transmission electron microscopy (TEM) (FEI/Philips Tecnai 12 BioTWIN). The Brunauer–Emmett–Teller (BET) surface area and pore size distribution were measured with an accelerated surface area and porosimetry system (ASAP 2010). Raman spectrum was recorded on a Renishaw RM-1000 Raman spectrometer with an excitation wavelength of 514 nm. X-ray photoelectron spectroscopy (XPS) measurements were performed on a KRATOS Axis ultra-DLD X-ray photoelectron spectrometer with a monochromatised Mg$K\alpha$ X-ray ($h\nu = 1283.3$ eV). Quantitative and qualitative analysis were carried out with a GC-FID (HP7890A with flame ionization detector, column HP5 30 m × 0.250 mm × 0.25 μm) and GC–MS (HP6890N with MSD5973, column HP5MS 30 m × 0.250 mm × 0.25 μm).

2.3. General procedure for selective oxidations of benzyl alcohol

Benzyl alcohol (1034 mg, 10.0 mmol) and 1 mol% of iron content in hematite core/shell spheres or other kinds of catalysts were added into a three-neck flask (about 50 mL) equipped with a condenser. The reaction mixture was vigorously stirred (500–750 rpm) at 75 °C. H_2O_2 (30 wt% in water, 1.0 mL, 10.0 mmol) was added continuously with a syringe pump in 12 h. The mixture was then cooled to room temperature and 1,4-dioxane (1760 mg, 20 mmol) was added as an internal standard for quantitative analysis by GC-FID. Three-time reproducibility testing showed the conversions of benzyl alcohol were in the range of 40–45%.

3. Result and discussion

3.1. Characterization of the samples

Fig. 1 shows a representative XRD pattern of the products prepared at various reaction times: (a) 1 h, (b) 12 h. Fig. 1a displays the typical XRD pattern of the as-prepared product, and all the peaks can be clearly indexed to a tetragonal phase of β-FeOOH (akaganeite) [space group: $I4/m$ (no. 87)], which are in good agreement with the literature values (JCPDS no. 13-157). Usually, β-FeOOH is regarded as the precursor of hematite. Fig. 1b shows a representative XRD pattern of hematite core/shell hierarchical structures. All the reflection peaks can be indexed to a pure rhombohedral phase of α-Fe_2O_3 (hematite) [space group: $R\bar{3}c$ (no. 167)], which are in good agreement with the literature values (JCPDS no. 72-469). The narrow sharp peaks indicates that the α-Fe_2O_3 product has good crystalline phase. No other phase can be detected from this pattern.

Raman spectroscopy is another useful technique to determine the surface conditions and homogeneity of crystalline or amorphous materials. The Raman spectrum of the typical sample is shown in Fig. 2a, which contains six bands at about 223, 239, 287, 401, 477 and 599 cm^{-1}. These peaks can be assigned to the $2A_{1g}$ and $3E_g$ Raman modes for the typical hematite phase.

Table 1
Experimental conditions for the preparation of some typical samples.

Sample no.	Reaction system	Solvothermal temperature (°C)	Reaction time (h)	Morphologies
1	5.0 g $FeCl_3 \cdot 6H_2O$ + 10.0 mL ethanol (2.0 mol L^{-1})	180	1	Nanorods
2	5.0 g $FeCl_3 \cdot 6H_2O$ + 10.0 mL ethanol (2.0 mol L^{-1})	180	2	Nanorods and solid spheres
3	5.0 g $FeCl_3 \cdot 6H_2O$ + 10.0 mL ethanol (2.0 mol L^{-1})	180	3	Solid spheres
4	5.0 g $FeCl_3 \cdot 6H_2O$ + 10.0 mL ethanol (2.0 mol L^{-1})	180	12	Hollow core/shell hierarchical nanostructures
5	5.0 g $FeCl_3 \cdot 6H_2O$ + 10.0 mL ethanol (2.0 mol L^{-1})	180	20	Broken hollow spheres
6	3.0 g anhydrous $FeCl_3$ + 10.0 mL ethanol (2.0 mol L^{-1})	180	12	Spheres composed of larger particles
7	0.5–1.5 g $FeCl_3 \cdot 6H_2O$ + 10.0 mL ethanol (0.2- 0.6 mol L^{-1})	180	12	200 nm solid particles
8	2.5 g $FeCl_3 \cdot 6H_2O$ + 10.0 mL ethanol (1.0 mol L^{-1})	180	12	500 nm solid particles
9	4.0 g $FeCl_3 \cdot 6H_2O$ + 10.0 mL ethanol (1.5 mol L^{-1})	180	12	500 nm hollow particles
10	5.5 g $FeCl_3 \cdot 6H_2O$ + 10.0 mL ethanol (2.2 mol L^{-1})	180	12	Assembly of core/shell hematite

XPS was used to determine the surface electronic states and the chemical composition of the product. In the high-resolution Fe 2*p* spectrum (Fig. 2b), the binding energies at 711.7 and 725.1 eV are the characteristic doublet from Fe 2*p*3/2 and Fe 2*p*1/2 core-level electrons, respectively. There is also a satellite at 719.8 eV, which is the characteristic peak of Fe(III) in Fe_2O_3 [61].

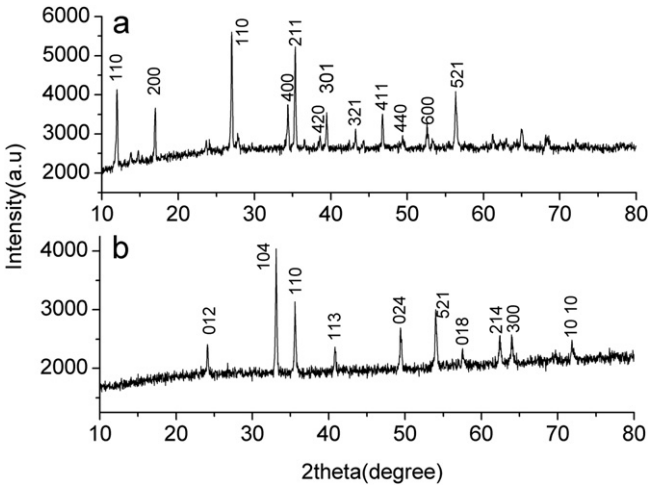

Fig. 1. XRD patterns of the samples obtained at different reaction time: (a) Sample 1, 1 h and (b) Sample 4, 12 h.

The morphologies of the samples were investigated with SEM and TEM. Fig. 3 shows the typical SEM micrographs of hematite. From Fig. 3a, one can see that the samples consist of sphere-like particles and parts of the particles have been broken. Fig. 3b shows the enlarged core/shell hierarchical structure, with ~200 nm shell thickness, and 1 μm of corresponding core diameter. The rough surface of the spheres implies that the surface of hematite spheres is composed of closely packed and well-aligned nanoparticles. In some conditions, some of the core/shell structures have been broken and the cores and shells have been completely or partly separated. Fig.3c gives the typical image of the cleaved cores, which are urchin-like spheres with porous tunnel. Hemispherical or bowl-shaped broken pieces with smooth surfaces and a shell thickness of 300 nm are also observed in SEM images.

TEM was used to further confirm the core/shell structure of the α-Fe_2O_3 core/shell spheres. Fig. 4a shows the representative TEM image of hematite. Fig. 4b is the broken shell of hematite, which shows the structural defects of the shell. The corresponding SAED pattern taken from an individual hematite sphere is shown in Fig. 4c. It can be seen that the assembled structure with micrometer-scale size almost exhibits a single-crystalline diffraction pattern.

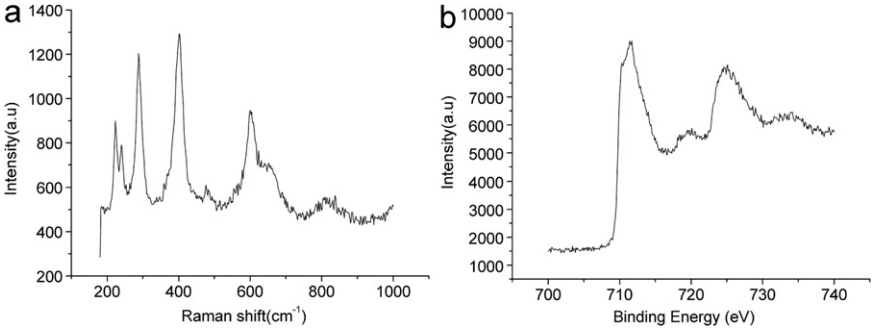

Fig. 2. (a) Raman spectrum of synthesized core/shell hierarchical hematite and (b) Fe 2p peaks in the XPS spectra (Sample 4).

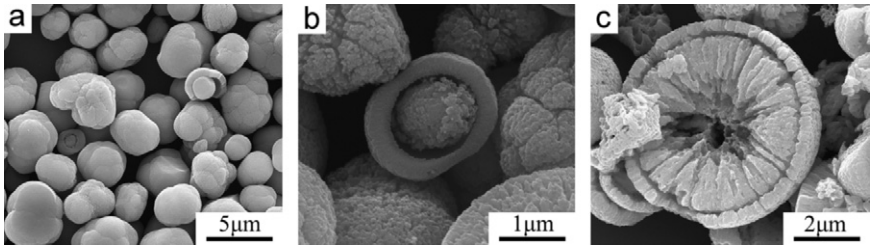

Fig. 3. Low (a) and high (b) magnification SEM images of the hierarchical hematite nanostructures and (c) High magnification SEM image of cleaved hematite core and shell (Sample 4).

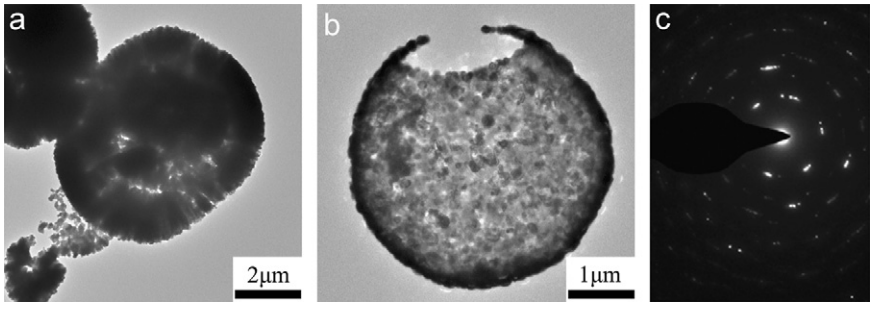

Fig. 4. (a) TEM image of typical core/shell structure of hematite, (b) TEM image of the separated shell of hematite and (c) selected area electron diffraction pattern taken from the shell (Sample 4).

Energy-dispersive X-ray analysis (EDAX) was also measured to determine the chemical composition of the ferrite samples. Results from EDAX spectrum (Fig. 5) showed that samples only contained Fe and O elements and the atomic ratio Fe/O was approximately 2:3, corresponding to α-Fe_2O_3.

Fig. 6 shows the nitrogen adsorption–desorption isotherm (Fig. 6a) and the pore size distribution curve (Fig. 6b) of the as-prepared core/shell hierarchical nanostructures of α-Fe_2O_3. It can be seen from Fig. 6 that the BJH (Barett–Joyner–Halenda) desorption average pore size and the BET surface area were 3.5 nm and 23.6 m^2/g, respectively, indicating the existence of nanoporous structures in the core/shell hierarchical nanostructures. The nanoporous structures provide communicable channels for chemical species traveling between the inner space of the nanostructures and the outer space of the solution, thus revealing the potential applications in a variety of fields. The porous nanostructures of the samples may have promising applications in catalysis since they can provide reactant substances with different size transport circumstance compared with those in open medium.

3.2. Effect of crystal water dissolved in the synthesis system

Since there was no surfactant or capping agent in our synthesis system, the ethanol employed in our synthesis was believed to act as both solvent and reactant during the formation of the core/shell hematite. In our previous work [56], etherification reaction of ethanol was found due to the existence of ethyl ether, which was further confirmed by Zeng group [52]. Although water from the etherification reaction may be vital for the hydrolysis of Fe^{3+} and the formation of the core/shell hematite, the crystal water molecules from $FeCl_3 \cdot 6H_2O$ in the reactant system is also necessary. In order to prove this hypothesis, anhydrous $FeCl_3$ was used as a substitute for $FeCl_3 \cdot 6H_2O$ with other conditions unchanged in the experiment. Fig. 7 shows the low and high magnification SEM images of the product obtained when anhydrous $FeCl_3$ was used instead of $FeCl_3 \cdot 6H_2O$. It can be clearly seen that solid spheres of about 10 μm were formed, which were self-assembled by small particles of ~500 nm. Under such condition, water content was greatly reduced and water from the etherification reaction was the only resource. So the hydrolysis rate of Fe^{3+} was dramatically decreased, leading to the formation of larger particles, and subsequently larger solid spheres.

3.3. Effect of Fe^{3+} concentration on the morphology

Besides the solvent, the effect of the Fe^{3+} concentration on the morphology of the precursor was also investigated. Keeping the volume of ethanol and other experimental conditions constant, the amount of $FeCl_3 \cdot 6H_2O$ was varied. Fig. 8a gives the SEM image of the sample obtained when 0.2–0.5 mol L^{-1} $FeCl_3 \cdot 6H_2O$ was used as starting material, which clearly showed that ~200 nm solid particles were the main products. Increasing the concentration to 1 mol L^{-1} the diameter of the particles increased to 500 nm (Fig. 8b). The surface of the particles was rough and consisted of small particles. From a large area, no broken particle can be observed. Further increasing the concentration to 1.5 mol L^{-1}, hollow nanostructure were obtained and the size of the particles was about 500 nm, as seen from the broken part of the hollow particles (Fig. 8c). When the concentration was above 2 mol L^{-1}, for example 2.2 mol L^{-1}, many core/shell hierarchical spheres tended to assemble together, going with the breakage of some spheres and the separation of parts of the cores from the shells (Fig. 8d).

3.4. Effect of reaction time on the morphology

In order to understand the formation process of the hierarchical core/shell hematite, we carried out time-dependent experiments

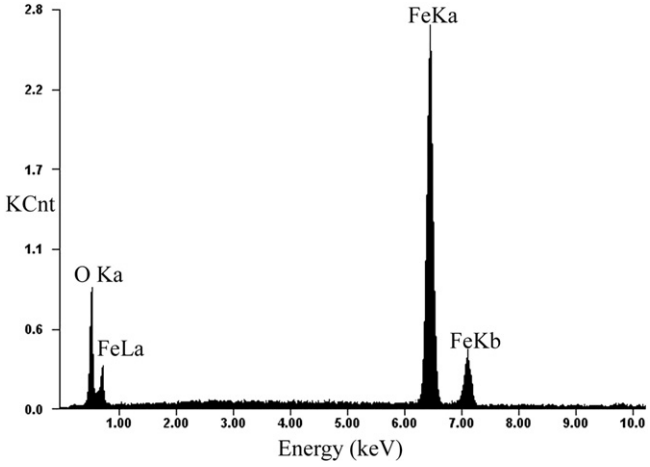

Fig. 5. EDAX spectrum of the prepared sample (Sample 4).

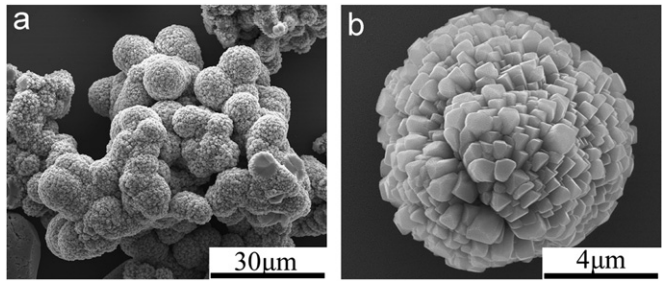

Fig. 7. Low (a) and high (b) magnification SEM image of hematite spheres prepared with anhydrous $FeCl_3$ and ethanol (Sample 6).

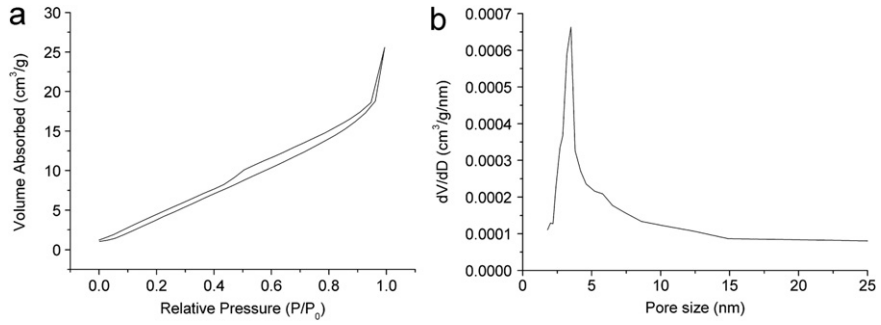

Fig. 6. (a) Nitrogen adsorption–desorption isotherm and (b) pore size distribution curve for the core/shell hierarchical hematite spheres (Sample 4).

during which samples were treated with different time. When the solvothermal reaction was conducted for 1 h, many needle-like particles were produced, whose diameter and length are about 20 nm and 2 μm (Fig. 9a). The particles presented yellow color and they were proved to be akaganeite phase (Fig. 1a). It is one of the most common existences of iron oxide in nature and usually regarded as the precursor of many kinds of iron oxides. When the reaction time was increased to 2 h, particles with thorns on their surface were observed, indicating that the particles were derived from the assembly of the nanorods, but incompletely formed (Fig. 9b). As the reaction went on for a longer time (e.g., 3 h), integrated assembly of solid spheres could be found (Fig. 9c). Fig. 9d shows the image of the core/shell hierarchical hematite prepared in 12 h. If the reaction time exceeded 12 h (e.g., 20 h), increasing core/shell structures were broken and separated from each other. At the same time, some particles diameters reached 10 μm and they became hollow spheres without cores (Figs. 9e and f).

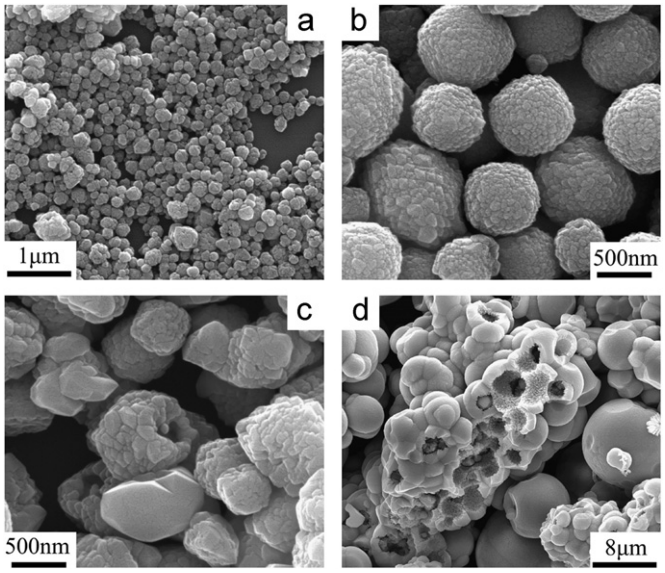

Fig. 8. SEM images of products obtained at different dosages of $FeCl_3$: (a) 0.50–1.5 g, (b) 2.5 g, (c) 4.0 g, (d) 5.5 g (Sample 7–10).

3.5. Formation mechanism of the core/shell hierarchical nanostructures

Considering the formation process of hollow interiors, it is categorized as the Ostwald ripening, which should be responsible for the forming mechanism of core/shell spheres. In general, Ostwald ripening involves the formation of aggregates with primary crystallites, followed by the gradual migration of crystallites through a recrystallization process due to the energy difference among them. Based on the time-dependent experiments, here, a two-step growth model is proposed for the formation of such a core/shell nanostructure. In the first step, as shown in Fig. 10, akaganeite nanorods first appeared in the solution after reaction for 1 h, and they might act as the primary particles for the formation of spheres. Through an Ostwald ripening process, these nanorods favored to aggregate together to form solid spheres, and then inner crystallites of the aggregate went to the outer shell through mass transfer. Meanwhile inner cores were formed by a dissolution–recrystallization process at the cost of small ones, which have higher surface energies and better solubility than the larger ones. Thus, core/shell hierarchical hematite spheres were obtained. With a prolonged ripening process, outward migration of crystals was dominant comparing with the inward one, resulting in the disappearance of the cores and thickening of the shells. Finally, hollow spheres with diameters of

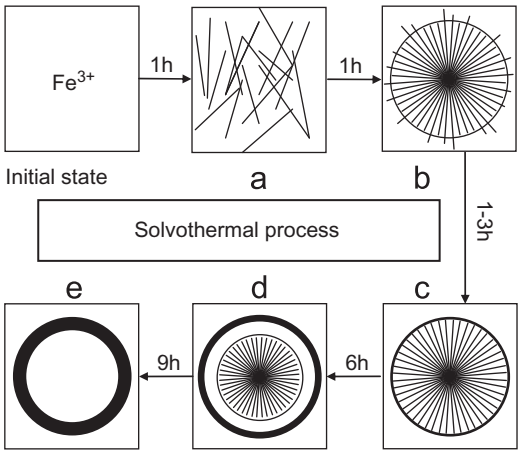

Fig. 10. Schematic illustration of the main process for the preparation of core/shell hierarchical hematite.

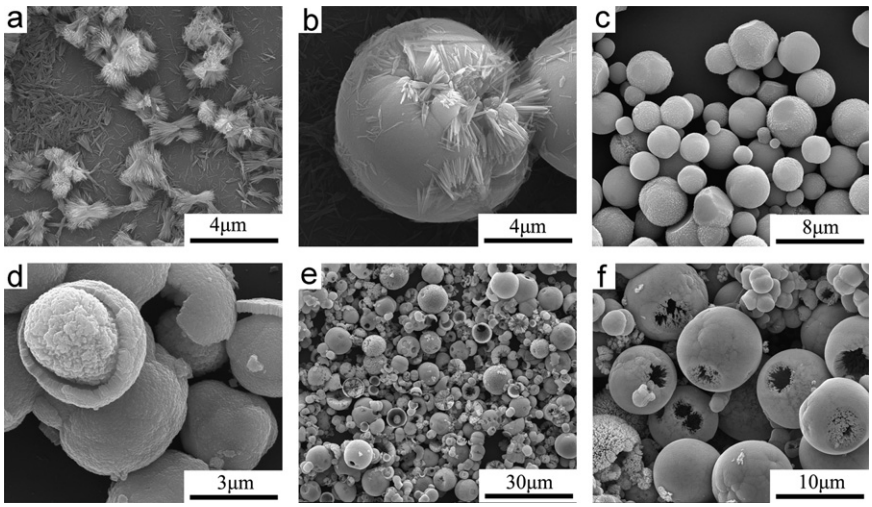

Fig. 9. Representative SEM images of six intermediaries: (a) 1 h, (b) 2 h, (c) 3 h, (d) 12 h, (e) and (f) 20 h (Sample 1–5).

Table 2
Selective oxidation of benzyl alcohol to benzaldehyde and benzoic acid.

Entry	Catalyst[a]	H_2O_2 (equiv.)	Conversion (%)	Selectivities (%)[b]	
				Benzaldehyde	Benzoic acid
1[c]	Bulk α-Fe_2O_3	1	7 ± 2	94	5
2[d]	Bulk γ-Fe_2O_3	1	8 ± 2	92	4
3[e]	Bulk Fe_3O_4	1	9 ± 2	93	3
4	$FeCl_3 \cdot 6H_2O$	1	89 ± 7	20	25
5	Sample 4	1	42 ± 3	95	2
6	Sample 4	1.5	60 ± 4	70	10
7[f]	Sample 4	1	41 ± 3	95	2

[a] 1 mol% of catalyst of iron content: 16 mg Fe_2O_3, 23 mg Fe_3O_4, 27 mg $FeCl_3 \cdot 6H_2O$.
[b] Benzaldehyde and benzoic acid were the only detectable products.
[c] Commercial hematite (particle size > 100 nm, solid spheres).
[d] It was obtained by annealing commercial magnetite in air at 250 °C for 3 h (particle size > 100 nm, solid spheres).
[e] Commercial magnetite (particle size > 100 nm, solid spheres).
[f] The catalyst was used after 5 times cycles.

about 10 μm were fabricated. The main process for preparing such core/shell structures was illustrated in Fig. 10.

3.6. Catalysis for the selective oxidation of benzyl alcohol to benzaldehyde

Herein, we used the as-prepared iron oxide to investigate their applications in organic synthesis. The oxidation of benzyl alcohol to benzaldehyde was chosen as model reaction. There have been papers about the optimal reaction conditions. The results for the selective oxidation are shown in Table 2, following the reported optimal reaction conditions [25,26].

In order to compare the different catalytic activities, several kinds of iron oxides were chosen as catalysts of the benzyl alcohol oxidation, including bulk α-Fe_2O_3, bulk γ-Fe_2O_3, bulk Fe_3O_4, $FeCl_3 \cdot 6H_2O$ and Sample 4. As expected, bulk α-Fe_2O_3, bulk γ-Fe_2O_3, bulk Fe_3O_4 (particle size > 100 nm) were poorly active and the conversions of benzyl alcohol were all below 10%, but the selectivities to benzaldehyde were all above 90% (Table 2, entries 1–3). $FeCl_3 \cdot 6H_2O$ is soluble in both water and benzyl alcohol and a homogeneous solution can be obtained. The reaction of hydrogen peroxide with ferric ions is referred to as a Fenton-like reaction [62]. Usually such reaction is non-selective radical reaction, during which the reactants are often over-oxidized and the products are beyond control. Under such condition, conversion of benzyl alcohol could reach its maximum, but the selectivity to benzaldehyde reached its minimum (Table 2, entry 4). High catalyst activity is achieved when Sample 4 (core/shell hierarchical structure) was applied. In this case, the conversion reached 42% together with 95% selectivity to benzaldehyde and 2% to benzoic acid (Table 2, entry 5). Adding more hydrogen peroxide (i.e. 1.5 equiv.) the conversion reached 60%, but selectivity to benzaldehyde decreased to 70% and to benzoic acid increased to 10% due to over oxidized (Table 2, entry 6). The reusability of the core/shell hierarchical spheres was carried out. No significant loss of catalyst activity is observed even after 5 times reuse (Table 2, entry 7).

Generally speaking, with increasing particle size of iron oxide, its catalytic activities decreased, while selectivity increased. The average diameter of core/shell hierarchical hematite spheres was around 4 μm, larger than that of the bulk hematite, but both the reaction activity and selectivity were high. Maybe the core/shell structures can count for the improved activity and selectivity. It is worth to notice that although the size of the core/shell spheres is ~4 μm, the pore size inside the core/shell structures is as small as ~3.5 nm. Benzyl alcohol or H_2O_2 molecules can get into the core/shell spheres through the pores, where they can meet and react with each other. Because there is large space for accommodating the reactant molecules inside the core/shell structures, the catalyst content is high enough in the local part of the core/shell spheres to obtain a high conversion and good selectivity to the final products.

4. Conclusion

In summary, hematite homogeneous core/shell hierarchical spheres were prepared through one-pot surfactant-free solvothermal treatment of $FeCl_3 \cdot 6H_2O$ and ethanol. High temperature (180 °C), high concentration (2.0 mol L^{-1}), crystal water of $FeCl_3$ and appropriate reaction time are key factors in conducting the synthesis. The Ostwald ripening formation process is confirmed by time-dependent experiments. XRD, Raman and EDAX are used to ascertain the composition of hematite. TEM and SEM images show that the products are composed of core/shell structures. XPS showed a satellite peak of Fe(III) at 719.8 eV. The size of the core/shell was ~4 μm and the shell thickness was ~300 nm. The oxidation of benzyl alcohol to benzaldehyde is chosen as model reaction, and it shows the enhanced catalytic activities of 42% conversion and 95% selectivity over the core/shell hematite catalyst.

Acknowledgment

This work was supported by the National Basic Research Program of China (973 Program) (no. 2010CB934500), the National Natural Science Foundation of China (NSFC) (nos. 51132006, 91027041, 21073127, 21071104, 20801010 and 20803008), A Foundation for the Author of National Excellent Doctoral Dissertation of PR China (FANEDD) (no. 200929). A Project Funded by the Priority Academic Program Development of Jiangsu Higher Education Institutions (PAPD).

References

[1] J.M. Du, J.L. Zhang, Z.M. Liu, B.X. Han, T. Jiang, Y. Huang, Langmuir 22 (2006) 1307.
[2] H.J. Choi, J.H. Shin, K. Suh, H.K. Seong, H.C. Han, J.C. Lee, Nano Lett. 5 (2005) 2432.
[3] Q.B. Wang, N. Iancu, D.K. Seo, Chem. Mater. 17 (2005) 4762.
[4] A. Prakash, A.V. McCormick, M.R. Zachariah, Nano Lett. 5 (2005) 1357.
[5] K. Kim, S. Webster, N. Levi, D.L. Carroll, M.R. Pinto, K.S. Schanze, Langmuir 21 (2005) 5207.
[6] D.P. Tang, R. Yuan, Y.Q. Chai, J. Phys. Chem. B 110 (2006) 11640.
[7] Z.C. Xu, Y.L. Hou, S.H. Sun, J. Am. Chem. Soc. 129 (2007) 8698.
[8] L.J. Lauhon, M.S. Gudiksen, C.L. Wang, C.M. Lieber, Nature 420 (2002) 57.
[9] S. Kar, S. Santra, H. Heinrich, J. Phys. Chem. C 112 (2008) 4036.
[10] C.W. Guo, Y. Cao, S.H. Xie, W.L. Dai, K.N. Fan, Chem. Commun. 39 (2003) 700.

[11] L. Zhu, X. Zheng, X. Liu, X. Zhang, Y. Xie, J. Colloid Interface Sci. 273 (2004) 155.
[12] Y.H. Zheng, Y. Cheng, Y.S. Wang, L.H. Zhou, F. Bao, C. Jia, J. Phys. Chem. B 110 (2006) 8284.
[13] I.D. Hosein, C.M. Liddell, Langmuir 23 (2007) 2892.
[14] B.P. Ha, L.A. Gao, J. Cryst. Growth 303 (2007) 616.
[15] B. Liu, H.C. Zeng, Small 1 (2005) 566.
[16] S.W. Cao, Y.J. Zhu, G.F. Cheng, Y.H. Huang, J. Phys. Chem. Solids 71 (2010) 1680.
[17] S.B. Ni, S.M. Lin, Q.T. Pan, F. Yang, K. Huang, X.Y. Wang, D.Y. He, J. Alloy Compd. 478 (2009) 876.
[18] R.M. Cornell, U. Schwertmann, The Iron Oxides: Structure, Properties, Reactions, Occurrences, Uses, Wiley-VCH Verlag GmbH & Co. KGaA, Weinheim, 2003.
[19] L.H. Huo, W. Li, L.H. Lu, H.N. Cui, S.Q. Xi, J. Wang, B. Zhao, Y.G. Shen, Z.H. Lu, Chem. Mater. 12 (2000) 790.
[20] W.T. Dong, C.S. Zhu, J. Mater. Chem. 12 (2002) 1676.
[21] R.H. Kodama, S.A. Makhlouf, A.E. Berkowitz, Phys. Rev. Lett. 79 (1997) 1393.
[22] C.Z. Wu, P. Yin, X. Zhu, C.Z. OuYang, Y. Xie, J. Phys. Chem. B 110 (2006) 17806.
[23] J.E. Bäckvall, Modern Oxidation Methods, Wiley-VCH Verlag GmbH & Co. KGaA, Weinheim, 2004.
[24] S.M. Roberts, Catalysts for Fine Chemical Synthesis, John Wiley & Sons, Ltd., England, 2007.
[25] F. Shi, M.K. Tse, M.M. Pohl, A. Brückner, S.M. Zhang, M. Beller, Angew. Chem. Int. Ed. 46 (2007) 8866.
[26] F. Shi, M.K. Tse, M.M. Pohl, J. Radnik, A. Brückner, S.M. Zhang, M. Beller, J. Mol. Catal. A-Chem. 292 (2008) 28.
[27] H. Firouzabadi, N. Iranpoor, M. Gholinejad, J. Hoseini, Adv. Synth. Catal. 353 (2011) 125.
[28] G.B. Yan, Y.B. Jiang, C.X. Kuang, S. Wang, H.C. Liu, Y. Zhang, J.B. Wang, Chem. Commun. 46 (2010) 3170.
[29] W. Zhang, J. Chen, X. Wang, H.L. Qi, K.S. Peng, Appl. Organomet. Chem. 23 (2009) 200.
[30] G. Sartori, R. Maggi, Chem. Rev. 106 (2006) 1077.
[31] T.J. Park, S.S. Wong, Chem. Mater. 18 (2006) 5289.
[32] Y.H. Zheng, Y. Cheng, Y.S. Wang, F. Bao, L.H. Zhou, X.F. Wei, Y.Y. Zhang, Q. Zheng, J. Phys. Chem. B 110 (2006) 3093.
[33] S.B. Wang, Y.L. Min, S.H. Yu, J. Phys. Chem. C 111 (2007) 3551.
[34] B.P. Jia, L. Gao, Cryst. Growth Des. 8 (2008) 1372.
[35] S. Hamada, E. Matijevic, J. Colloid Interface Sci. 84 (1981) 274.
[36] X.L. Hu, J.C. Yu, J.M. Gong, Q. Li, G.S. Li, Adv. Mater. 19 (2007) 2324.
[37] S.L. Zhong, J.M. Song, S. Zhang, H.B. Yao, A.W. Xu, W.T. Yao, S.H. Yu, J. Phys. Chem. C 112 (2008) 19916.
[38] Y.L. Chueh, M.W. Lai, J.Q. Liang, L.J. Chou, Z.L. Wang, Adv. Funct. Mater. 16 (2006) 2243.
[39] X.G. Wen, S.H. Wang, Y. Ding, Z.L. Wang, S.H. Yang, J. Phys. Chem. B 109 (2005) 215.
[40] S.Y. Lian, E.B. Wang, Z.H. Kang, Y.P. Bai, L. Gao, M. Jiang, C.W. Hu, L. Xu, Solid State Commun. 129 (2004) 485.
[41] J.J. Wu, Y.L. Lee, H.H. Chiang, D.K.P. Wong, J. Phys. Chem. B 110 (2006) 18108.
[42] L. Vayssieres, C. Sathe, S.M. Butorin, D.K. Shuh, J. Nordgren, J.H. Guo, Adv. Mater. 17 (2005) 2320.
[43] K. Woo, H.J. Lee, J.P. Ahn, Y.S. Park, Adv. Mater. 15 (2003) 1761.
[44] C.J. Jia, L.D. Sun, Z.G. Yan, L.P. You, F. Luo, X.D. Han, Y.C. Pang, Z. Zhang, C.H. Yan, Angew. Chem. Int. Ed. 44 (2005) 4328.
[45] L. Liu, H.Z. Kou, W.L. Mo, H.J. Liu, Y.Q. Wang, J. Phys. Chem. B 110 (2006) 15218.
[46] C.J. Jia, L.D. Sun, Z.G. Yan, Y.C. Pang, L.P. You, C.H. Yan, J. Phys. Chem. C 111 (2007) 13022.
[47] C.R. Gong, D.R. Chen, X.L. Jiao, Q.L. Wang, J. Mater. Chem. 12 (2002) 1844.
[48] M.V. Reddy, T. Yu, C.H. Sow, Z.X. Shen, C.T. Lim, G.V.S. Rao, B.V.R. Chowdari, Adv. Funct. Mater. 17 (2007) 2792.
[49] Y.W. Zhu, T. Yu, C.H. Sow, Y.J. Liu, A.T.S. Wee, X.J. Xu, C.T. Lim, J.T.L. Thong, Appl. Phys. Lett. 87 (2005) 023103.
[50] D.B. Wang, C.X. Song, G.H. Gu, Z.S. Hu, Mater. Lett. 59 (2005) 782.
[51] L.S. Zhong, J.S. Hu, H.P. Liang, A.M. Cao, W.G. Song, L.J. Wan, Adv. Mater. 18 (2006) 2426.
[52] S.Y. Zeng, K.B. Tang, T.W. Li, Z.H. Liang, D. Wang, Y.K. Wang, Y.X. Qi, W.W. Zhou, J. Phys. Chem. C 112 (2008) 4836.
[53] C. Jia, Y. Cheng, F. Bao, D.Q. Chen, Y.S. Wang, J. Cryst. Growth 294 (2006) 353.
[54] X.L. Hu, J.C. Yu, J.M. Gong, J. Phys. Chem. C 111 (2007) 11180.
[55] S.W. Cao, Y.J. Zhu, J. Phys. Chem. C 112 (2008) 12149.
[56] S.Y. Lian, E.B. Wang, L. Gao, D. Wu, Y.L. Song, L. Xu, Mater. Res. Bull. 41 (2006) 1192.
[57] L.L. Li, Y. Chu, Y. Liu, L.H. Dong, J. Phys. Chem. C 111 (2007) 2123.
[58] J.H. Bang, K.S. Suslick, J. Am. Chem. Soc. 129 (2007) 2242.
[59] B.D. Mao, Z.H. Kang, E.B. Wang, C.G. Tian, Z.M. Zhang, C.L. Wang, Y.L. Song, M.Y. Li, J. Solid State Chem. 180 (2007) 489.
[60] G.M. Whitesides, M. Boncheva, Proc. Natl. Acad. Sci. USA 99 (2002) 4769.
[61] T.J. Daou, G. Pourroy, S. Bégin-Colin, J.M. Grenèche, C. Ulhaq-Bouillet, P. Legaré, P. Bernhardt, C. Leuvrey, G. Rogez, Chem. Mater. 18 (2006) 4399.
[62] C. Walling, A. Goosen, J. Am. Chem. Soc. 95 (1973) 2987.